Journal of Materials Chemistry A

3D Activated Microporous Protective Layer for High-Energy Lithium Metal Batteries

Journal:	*Journal of Materials Chemistry A*
Manuscript ID	TA-ART-11-2024-007861.R1
Article Type:	Paper
Date Submitted by the Author:	14-Jan-2025
Complete List of Authors:	Lee, Kyungbin; Georgia Institute of Technology, Mechanical Engineering Kim, Hyojin; Korea Research Institute of Chemical Technology; Seoul National University, Ryu, Kun; The University of Chicago, Pritzker School of Molecular Engineering; Argonne National Laboratory, Chemical Sciences and Engineering Division Kim, Keun-Hee; Georgia Institute of Technology, Mechanical Engineering Jeon, Jun Woo; Korea Institute of Science and Technology Lee, Michael; Kyung Hee University, Mechanical Engineering Kim, Soohyun; LG Energy Solution Kim, Dayoung; LG Energy Solution Shin, Dongseok; LG Energy Solution Kim, Byoung Gak; Korea Research Institute of Chemical Technology, Lee, Seung Woo; Georgia Institute of Technology, School of Mechanical Engineering

ARTICLE

3D Activated Microporous Protective Layer for High-Energy Lithium Metal Batteries

Received 00th January 20xx,
Accepted 00th January 20xx

DOI: 10.1039/x0xx00000x

Kyungbin Lee,[a,†] Hyojin Kim,[b,†] Kun Ryu,[a,c,d,†] Keun Hee Kim,[a,†] Jun Woo Jeon,[e] Michael J. Lee,[a,f] Soohyun Kim,[g] Dayoung Kim,[g] Dongseok Shin,[g] Byoung Gak Kim[b,h,*], and Seung Woo Lee[a,*]

For the operation of rechargeable lithium (Li) metal batteries (LMBs), ensuring the stability and efficiency of Li metal anodes (LMAs) is crucial. The solid-electrolyte interphase (SEI) plays a pivotal role in this context, but its dynamic and often inconsistent nature poses significant challenges, leading to uncontrollable Li dendrite growth and potential short-circuit. To address these challenges, we introduce an activated microporous protective layer designed to stabilize LMAs. This protective layer not only effectively suppresses electrolyte consumption but also enhances passivation properties, ensures homogeneity, and mechanical integrity during cycling. Leveraging these unique characteristics, we achieve high-efficiency Li deposition and stable cycling with Li iron phosphate ($LiFePO_4$, 3.9 mAh cm^{-2}) and high-nickel ($LiNi_{0.83}Mn_{0.06}Co_{0.11}O_2$, 3 mAh cm^{-2}) cathodes, even under demanding conditions such as high-loading cathodes and limited lithium excess. This research contributes to advancing more reliable and efficient high-energy LMBs, addressing critical challenges in energy storage technology.

Introduction

Lithium (Li) metal anodes hold substantial promise in rechargeable battery technology due to their superior theoretical specific capacity (3,860 mAh g^{-1}).[1] However, intrinsic challenges associated with Li metal anodes (LMA) limit the practical application of Li metal batteries (LMBs).[2] These challenges include uncontrollable Li corrosion, an unstable solid-electrolyte interphase (SEI), and the formation of inactive metallic Li^0 from highly tortuous dendrites, which contribute to low Li irreversibility and the loss of Li inventory in LMBs.[3, 4] Various approaches have been investigated to enhance the performance of LMA, including the design of novel electrolytes,[5-8] reduction of initial nucleation overpotential using lithiophilic metal-embedded frameworks,[9, 10] and the creation of an artificial interlayer on the surface of LMA.[11] One practical strategy involves applying an artificial polymeric layer, which offers benefits such as low cost, facile synthesis, and scalability.[12, 13] Furthermore, the tunable chemistry and improved mechanical attributes of polymers provide robust protection to LMA.[14]

A polymeric interlayer ideally must fulfill several functional roles similar to those of the native SEI: maintaining high ionic conductivity and low electronic conductivity, demonstrating enhanced electrochemical stability and robust mechanical strength, preventing dendrite growth, and remaining compatible with the liquid electrolyte.[15, 16] Polymers inherently possess superior mechanical properties due to their molecular network structures, enabling them to accommodate volume changes and fortify the Li-electrolyte interface by isolating the highly reactive LMA.[13, 17] However, conventional soft polymers face limitations in fulfilling these roles due to their limited ionic conductivity and electrochemical stability.[18, 19] To overcome these challenges, two major strategies have been explored: developing inorganic/organic composite layers[20-23] and bi-layered SEIs.[24-27] However, these methods are typically suitable only for limited operation under low current densities.[28-30] Thus, there is a significant demand for an interlayer with high ionic conductivity and electrochemical stability that can facilitate dendrite-free Li deposition under realistic conditions.

Recently, polymers of intrinsic microporosities (PIMs) have emerged as an effective method to achieve stable and compact Li deposition.[31-34] These polymers feature ion solvation cages with pore widths of approximately 9 Å, selectively permeating Li^+ ions and increasing their availability at the electrochemical double layer.[31, 34] The accumulation of surplus Li^+ ions in the vicinity of the LMA enhances the Li^+ transference number (t_{Li}), thereby mitigating diffusion-induced constraints during Li deposition. By alleviating diffusion-limited reduction at the

[a.] George W. Woodruff School of Mechanical Engineering, Georgia Institute of Technology, Atlanta, GA 30332, USA.
[b.] Advanced Materials Division, Korea Research Institute of Chemical Technology (KRICT), 141 Gajeong-ro, Yuseoung-gu, Daejeon 34114, Republic of Korea.
[c.] Pritzker School of Molecular Engineering, University of Chicago, Chicago, IL 60637, USA
[d.] Chemical Sciences and Engineering Division, Argonne National Laboratory, Lemont, IL 60439, USA
[e.] Institute of Advanced Composite Materials, Korea Institute of Science and Technology (KIST), 92 Chudong-ro, Bongdong-eup, Wanju-gun, Jeonbuk, 55324, Republic of Korea
[f.] Department of Mechanical Engineering, College of Engineering, Kyung Hee University, Yongin 17104, Republic of Korea.
[g.] LG Energy Solution, Ltd., LG Science Park, Seoul 07796, Korea
[h.] Department of Chemical Convergence, Materials and Process, University of Science and Technology, Daejeon 34114, Republic of Korea
† These authors contributed equally to this work.
Supplementary Information available: [details of any supplementary information available should be included here]. See DOI: 10.1039/x0xx00000x

electrode surface, PIMs have demonstrated prolonged cell cycle life, characterized by dendrite-free compact Li deposition morphologies. In particular, a recent study introduced a universal chemomechanical model that delineates the conditions under which solid ion conductors (SICs) can suppress dendrite formation.[32] The SIC with high shear modulus effectively blocked dendrite propagation using pressure-driven mechanisms, while the low shear modulus demonstrated dendrite suppression through density-driven stability. Inspired by this study, we aimed to investigate alternative strategies that promotes uniform Li electrodeposition with improved mechanical properties to accommodate the significant volume changes at the LMA.

In this study, we introduce a 3D microporous artificial polymer interlayer designed for the LMA, aimed at achieving stable cycling even under high current densities and areal capacities (Fig. 1). Our interlayer design utilizes highly carboxylate-functionalized PIM (PCH) crosslinked with poly(ethylene glycol) diglycidyl ether (PEGDE) to form a robust and ion-conducting polymeric interlayer. The resulting PIM-COOH crosslinked with PEGDE (PCHP) demonstrates improved t_{Li} (0.74), mechanical strength (Young's modulus = 3.85 GPa), and electrochemical stability. Particularly noteworthy is the observed chemo-mechanical conversion of PCHP, transitioning from COOH to COOLi, indicative of an (electro)chemically stable interface. The full cell incorporating a PCHP-coated 35 µm thick Li anode and a 2.8 mAh cm^{-2} $LiFePO_4$ (LFP) cathode shows excellent capacity retention of 93% after 500 cycles at a high current density of 2 mA cm^{-2}. Similarly, using a 3 mAh cm^{-2} $LiNi_{0.83}Co_{0.11}Mn_{0.06}O_2$ (NCM83) cathode configuration, the cell exhibits 76% capacity retention after 400 cycles under the same high current density of 2 mA cm^{-2}).

Results and discussion

In our previous study, we obtained PCH through the alkaline hydrolysis of the cyano group in PIM-1 to carboxylic acid, which readily react with the epoxide ring.[35] The synthesis of PCH in this study followed the methodology established in our earlier research.[35] The conversion of nitrile groups to carboxylic acid groups was confirmed via nuclear magnetic resonance (NMR) and elemental analysis (EA), revealing an approximately 92% conversion rate (Fig. S1 and Table S1). The conversion rate was calculated using a previously established method.[35] The detailed calculation method for determining the conversion rate has been provided in the Supporting Information to enhance clarity and reproducibility. The ^{1}H NMR analysis conducted in DMSO-d6 (Fig. S1) identified characteristic peaks corresponding to the aromatic backbone (6–7 ppm) and carboxylic acid (-COOH) functional groups (13–14 ppm), confirming the successful conversion of nitrile (CN) to COOH groups. To enhance both the mechanical properties and ion conductivity of PCH, we utilized PEGDE as a cross-linking agent. The formulations cross-linked with PEGDE were named PCHP, PCHP2, and PCHP3, corresponding to PIM-COOH and PEGDE ratios of 2:1, 1:1, and 1:2, respectively. Solid-state ^{13}C NMR analysis was performed to investigate the chemical transformations in PEGDE, PCH, and their crosslinked derivatives (PCHPs) (Fig. S2). The disappearance of the epoxide ring peak (40–50 ppm) and the appearance of new methylene peaks (70–80 ppm) confirmed the reaction between PCH and PEGDE. Additionally, the presence of a small broad peak near 160 ppm in PCHPs, corresponding to unreacted COOH groups, suggests that not all COOH groups reacted with PEGDE and that some self-reaction of PEGDE may have occurred.[36, 37]

Differential Scanning Calorimetry (DSC) analysis, as shown in Fig. 2(a), was performed to investigate the thermal properties of PCH, its crosslinked derivatives (PCHP, PCHP2, and PCHP3), and comparison samples such as PEO 200K and PEGDE. The measurements, conducted over a range of -30°C to 180°C, revealed distinct differences in thermal behavior. While PEO exhibited clear melting transitions (Tm) due to its crystalline nature, PCHPs showed no such transitions. This observation indicates that the PEGDE crosslinking effectively disrupts crystallization within the polymer matrix, enhancing its amorphous character. Furthermore, the absence of crystallization in PCHPs is consistent with their improved ion transport properties and ability to accommodate volume changes during cycling. The intrinsic microporosity of PIMs enables PCHP to act as sieves and ion solvation cages, facilitating the selective permeation of Li^+ ions.[31, 38, 39] CO_2 sorption isotherms and X-ray diffraction (XRD) measurements of PCH and PCHPs were conducted to investigate changes in the pore structure of PCHP following the cross-linking reaction. In Fig. 2b, the average interchain distances, or d-spacings, were calculated using Bragg's law ($d = \lambda/(2\sin\theta)$), based on the maximum 2θ values from the broad peaks observed. In PCH, d-spacings of 4.87 and 6.92 Å were identified. The d-spacing of 4.87 Å reflects the distance between polymer chains aligned in a chain-to-chain configuration. The broader band at 6.92 Å suggests the presence of more loosely packed polymer chains due to intrinsic microporosity. The slight decrease in d-spacings can be attributed to the reduced distances between polymer chains from

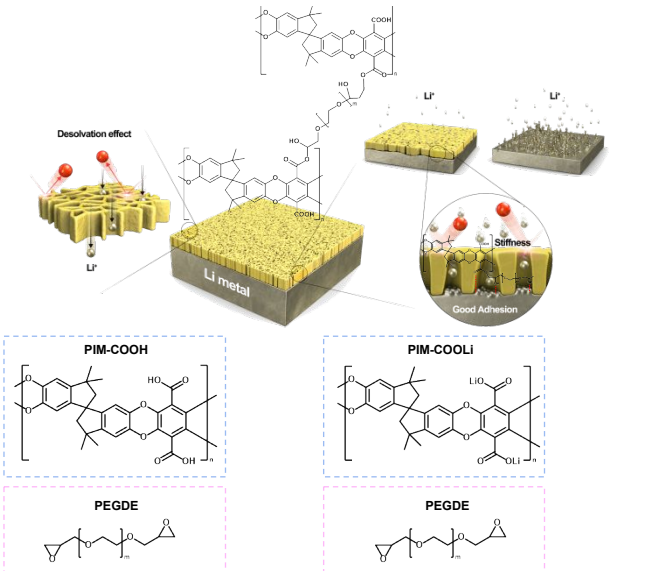

Fig. 1 Schematic illustration and design of the 3D activated microporous protective layer (PCHP).

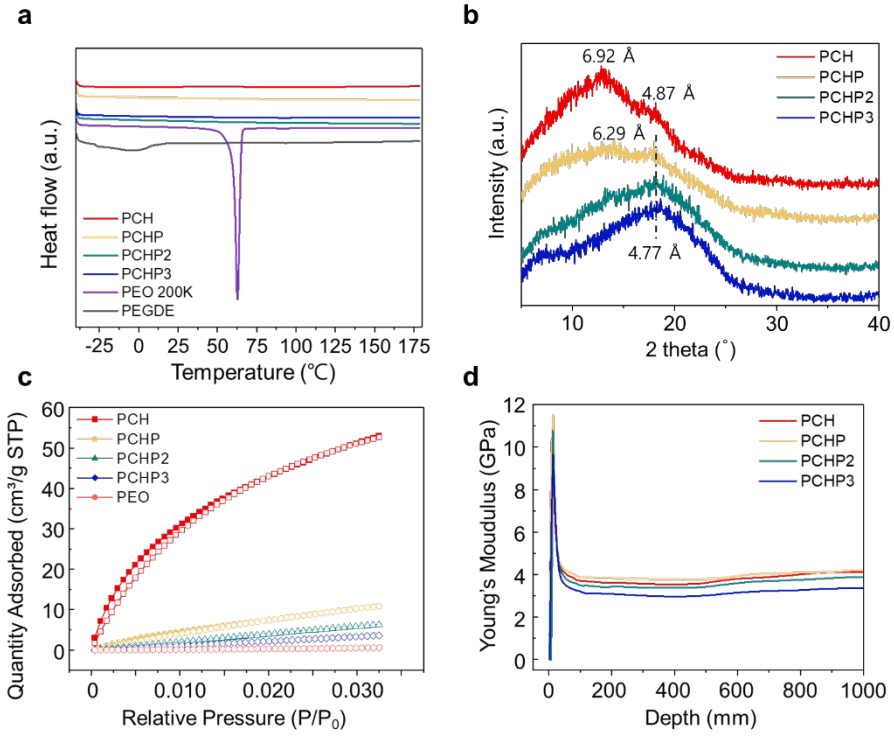

Fig. 2 (a) DSC curves, (b) XRD results, (c) CO_2 sorption isotherm at 277K, and (d) nanoindentation analysis of PCH and PCHP.

cross-linking.[35, 40, 41] Notably, in PCHP2 and PCHP3, the peaks associated with microporosity in the 6 to 7 Å range disappeared, as observed in the CO_2 sorption isotherms (Fig. 2c, Fig. S3 and Table S2). While CO_2 sorption isotherms at 227K for PCHP showed a significant decrease compared to PCH, XRD results indicated that the microporosity was maintained. Fig. S3 features a magnified graph of CO_2 sorption isotherms for PCHPs, illustrating a curve characteristic of microporosity, unlike the non-porous PCHP2, PCHP3, and polyethylene oxide.[35 42] When the reduction in distances between PCH polymer chains exceed 50% cross-linked content, the microporosity characteristics are lost, diminishing the facilitation of Li^+ ion mobility.

To evaluate the mechanical properties critical for inhibiting Li dendrite formation, nanoindentation measurements were conducted. The results depicted in Fig. 2d demonstrate that after cross-linking, the Young's modulus of PCH (3.46 GPa)

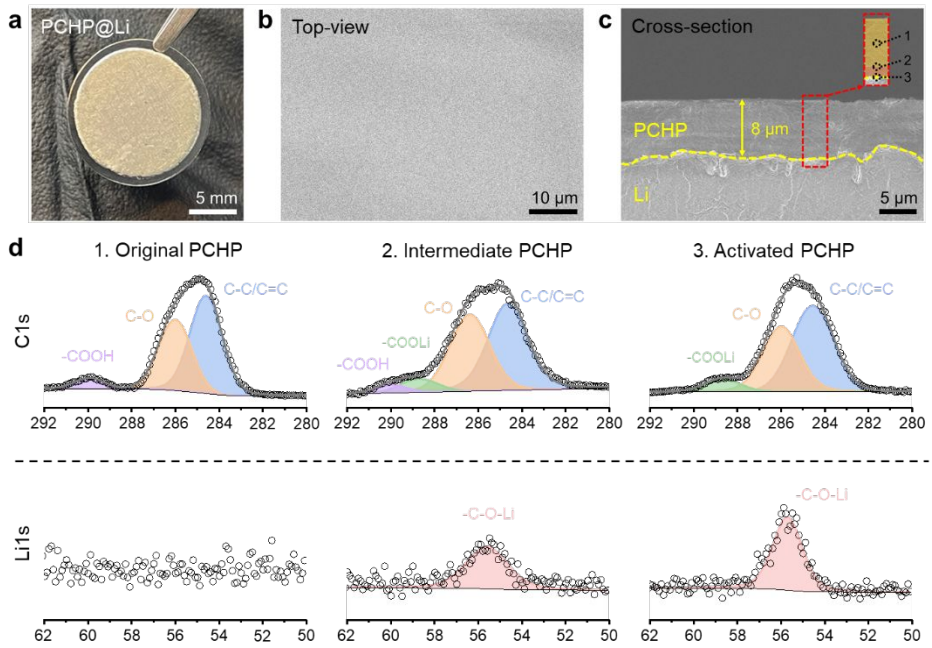

Fig. 3 (a) Physical image, (b) Top-view SEM, and (c) Cross-section view SEM of PHCP@Li (Inset: location of XPS analysis). (d) High-resolution C 1s and Li 1s XPS of different layers of PCHP.

improved to PCHP (3.85 GPa). However, as the ratio of the cross-linker increased further, the mechanical properties gradually decreased due to the influence of the flexible ether groups, with PCHP2 and PCHP3 exhibiting values of 3.26 GPa and 3.08 GPa, respectively. Each of the PCH and cross-linked PCHP polymers exhibited Young's modulus values exceeding 3 GPa, demonstrating their sufficient mechanical strength to effectively suppress the formation of lithium dendrites.[22] To further investigate the role of the PEGDE crosslinker in adhesive properties, we assessed the differences in interfacial adhesion between PCH and PCHP with electrodes. Thin coatings of each polymer solution were applied to copper foils, which were then examined via scanning electron microscope (SEM) and subjected to peel tests using a Universal Testing Machine (UTM) (Fig. S4). The inherently rigid structure of PCH caused delamination from the copper foil during drying, resulting in interfacial voids. In contrast, PCHP, enhanced by flexible PEGDE cross-linking, formed a seamless interface with the copper foil. Average adhesive strength of PCHP was approximately twice that of PCH, with notably uniform adhesion. This highlights the effectiveness of PEGDE crosslinking in improving interfacial adhesion.

PCHP coated on the LMA was identified as the optimal composition for stabilizing LMAs based on the previous screening process (Fig. 3a). Both top-view and cross-sectional SEM image showed that the PCHP layer was uniformly coated on the LMA with a thickness of 8 μm (Fig. 3b, c). We hypothesize that the PCH-based polymer SEI can serve as a passivating layer after a direct activation process. Activation of PCHP can be achieved by a one-step chemical reaction on the Li surface, where carboxylate groups from PCH react with Li to form CO_2-Li, which can provide enhanced ionic conduction and active channels for Li-ion transfer.[12, 43] We classified the PCHP into three different layers: original PCHP (comprising 100% of the PCHP layer), intermediate PCHP (a mixture of original PCHP and activated PCHP layer), and activated PCHP. Fig. 3d shows deconvoluted high-resolution X-ray photoelectron spectroscopy (XPS) spectra of these three layers. Original PCHP exhibited C-C/C=C bonds (284.5 ± 0.2 eV in C 1s), C-O bonds (285.9 ± 0.2 eV), and -COOH bonds (290.2 ± 0.2 eV). In the intermediate PCHP layer, new -COOLi bonds (288.9 ± 0.2 eV) were observed alongside -COOH bonds. Notably, in the activated PCHP layer (near the Li surface), -COOH bonds were fully converted to -COOLi bonds. In addition, the emergence and increased intensity of -C-O-Li bonds in the Li 1s spectrum (55.7 eV) further corroborate the conversion of -COOH bonds to -COOLi bonds through the chemical reaction between PCH and Li surface.

We evaluated the stability of LMA by testing Li||Li symmetric cells at a current density and areal capacity of 1 mA cm^{-2} and 1 mAh cm^{-2}, respectively (Fig. 4a). The symmetric cell with bare Li anodes exhibited increased overpotential and severe voltage fluctuations, leading to cell failure within 344 hours. In contrast, the PCHP-coated Li anode (PCHP@Li) demonstrated stable Li plating/stripping behavior, maintaining a low polarization of 26 mV after an extended duration of 1000 hours. Additionally, the PCHP@Li anode showed outstanding stability over 1000 hours compared to the bare Li anode, even at a high current density of 3 mA cm^{-2} and an areal capacity of 3 mAh cm^{-2} (Fig. S5). To understand the underlying mechanism behind the improved stability with the PCHP coating, Li symmetric cells were cycled under identical conditions for 50 and 100 cycles, followed by SEM analysis. SEM images in Fig. 4b show mossy and highly porous Li deposits on the surface of the bare LMA. On the other

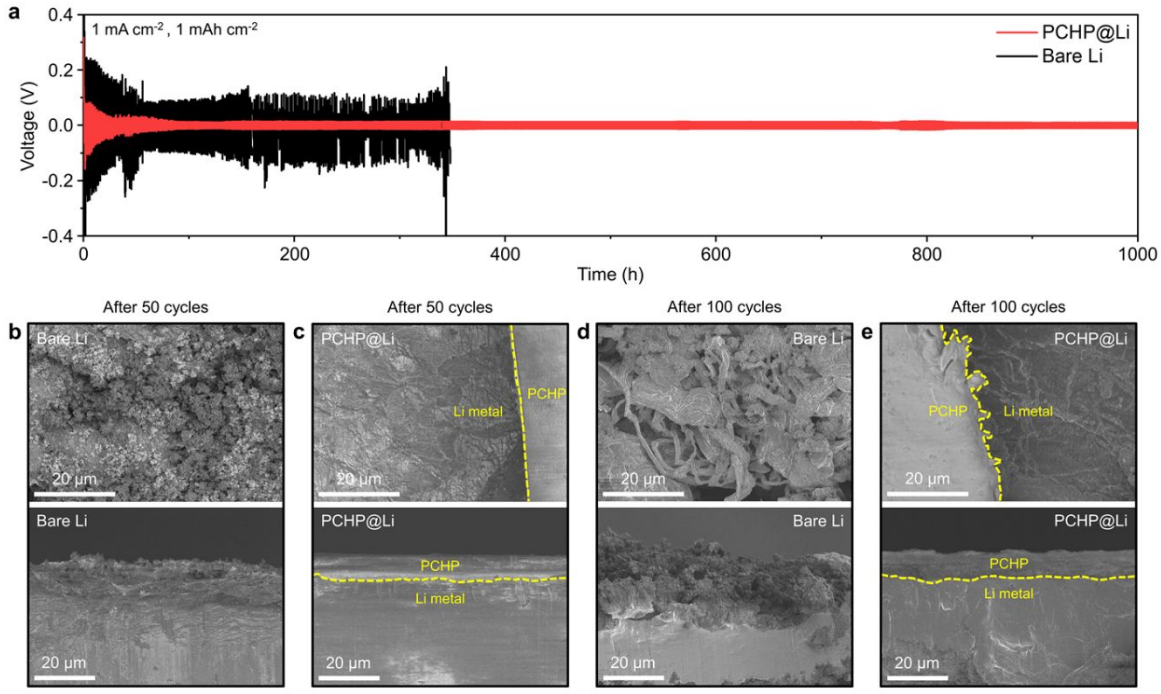

Fig. 4 (a) Cycling stability of Li|Li symmetric cells at 1 mA cm^{-2} and 1 mAh cm^{-2}. SEM images illustrating the surface morphology and cross-sectional views of cycled LMA after 50 and 100 cycles (b, d) Li and (c, e) PCHP@Li cycled at 1 mA cm^{-2} and 1 mAh cm^{-2}.

hand, PCHP@Li exhibited uniform lithium deposits, indicating enhanced protection from PCHP (Fig. 4c). After 100 cycles, rod-like dendrites were observed on the surface of the bare LMA (Fig. 4d). The cross-sectional morphology displayed a thick layer of SEI and inactive Li. Conversely, PCHP@Li maintained smooth and compact Li deposition, consistent with observations made in the SEM images (Fig. 4e). This highlights the role of PCHP in improving the long-term operational stability and cyclability of LMAs. Furthermore, the C1s XPS spectrum of PCHP after 100 cycles revealed no significant chemical degradation within PCP (Fig. S6), supporting the robustness of this material for LMA applications. To further investigate the interfacial resistance of bare Li and PCHP@Li, electrochemical impedance spectroscopy measurements of Li symmetric cells were conducted before and after 20, 40, and 60 cycle, respectively (Fig. S7). During cycling, the overall impedance of bare Li increased due to the development of an SEI layer on the dendritic growth of the Li surface. Interestingly, the charge transfer resistance of PCHP@Li decreased upon cycling. This was attributed to the enhanced ion transport channels of activated PCHP and the encapsulation of electrolytes within the nanopores of non-activated PCHP.[32] Furthermore, the Li-ion transference number (t_{Li+}) was evaluated to assess the proportion of ion current carried by Li-ion when confined with the PCHP layer in Li||Li symmetric cells (Fig. S8).[44] Using the Bruce-Vincent method, a t_{Li+} of 0.74 was determined, whereas the reference cell with only a Celgard separator showed a t_{Li+} of 0.28.[44] This suggests that the PCHP layer effectively limits space-charge accumulation in the SEI during high-rate Li metal plating, thereby significantly enhancing performance under lager constant current operation.

To demonstrate the performance rechargeable LMBs under realistic conditions, we tested LMBs with a 35 µm thick LMA and high-loading cathodes of NCM83 and LFP (Fig. 5a). Rate capability analysis was performed on NCM83 cathodes with loadings of 3.0 mAh cm^{-2} at current densities ranging from 0.1 to 5.0 mA cm^{-2} (Fig. 5b, 5c, and S9). PCHP@Li demonstrated superior rate performance, particularly evident at 5.0 mA cm^{-2} where PCHP@Li maintained a higher capacity (90.2 mAh g^{-1}) than bare Li (32.4 mAh g^{-1}). We further proceeded fabricating a full cell to examine the cycling stability of PCHP@Li anode (Fig. 5d and S10). The full cell employing PCHP@Li exhibited an impressive capacity retention of 76% (compared to 3rd cycle capacity) after 400 cycles with an average Coulombic efficiency (CE) of 99.85%. It is worth noting that this cell was cycled at 2 mA cm^{-2}, corresponding to a high rate of 0.66 C. In contrast, the bare Li||NCM83 full cell encountered failure within 200 cycles, indicating the loss of Li reservoir within the full cell. We also evaluated full cells consisting of thin Li (35 µm) and high loading LFP cathode (16.3 mg cm^{-2}, or 2.8 mAh cm^{-2}), which were cycled at a high current density of 2 mA cm^{-2} (equivalent to 0.71 C, Fig. 5e and S11). The cell employing PCHP@Li exhibited a high capacity retention of 93% (compared to 3rd cycle capacity) after 500 cycles with an average CE of 99.95%. In contrast, bare Li anodes showed a capacity retention of 78.6% after 200 cycles and ultimately short-circuited after 275 cycles. To further verify the feasibility of our findings, we conducted

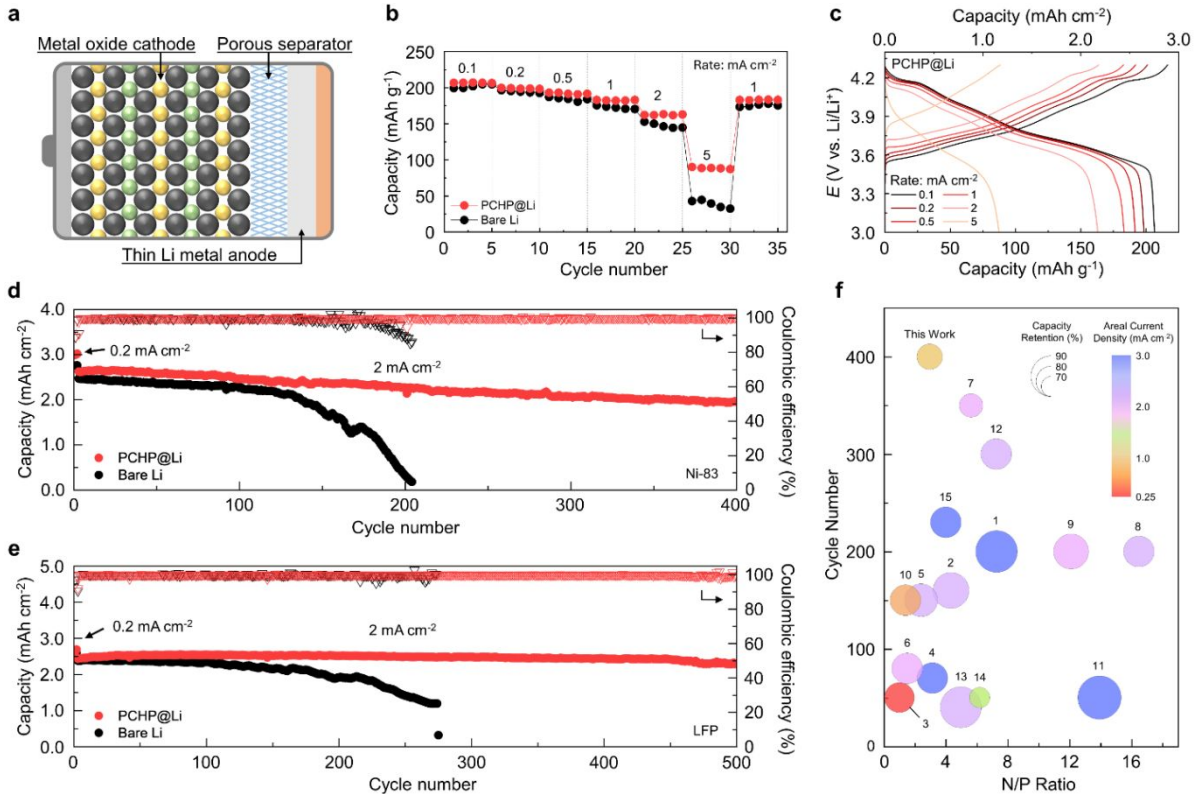

Fig. 5 (a) Schematic of LMBs with a thin LMA and high loading cathode. (b) Rate-performance of the full cell with bare Li and PCHP@Li anode at different areal current densities. (c) Corresponding charge/discharge profiles of the full cell with PCHP@Li anode. Cycling performance of the full cell with (d) high loading LFP cathode and (e) NCM83 cathode at 2 mA cm^{-2}. (f) Comparison of full cell performance with previously reported studies in terms of N/P ratio, cycle number, capacity retention, and areal current density.

additional tests with higher loading LFP cathodes. The 35 μm-thick LMA was paired with 23.1 mg cm^{-2} (or 3.9 mAh cm^{-2}) LFP cathode and were cycled at a current density of 3 mA cm^{-2} (Fig. S12). The cell with PCHP@Li displayed a capacity of 124 mAh g^{-1} after 300 cycles, corresponding to a capacity retention of 84%, highlighting the prominent role of PCHP in achieving high LMB cyclability. The pronounced difference in electrochemical performance highlights the pivotal role of PCHP in ensuring high reversibility and stability of LMA, particularly in conditions with limited Li inventory. Our PCHP design outperforms other state-of-the-art coating strategies in terms of cycle life and N/P ratio, representing a significant advancement in the development of high-energy LMBs (Fig. 5f).[1-6, 9-17]

Conclusions

This study introduces a 3D microporous artificial polymer interlayer designed to stabilize LMAs. By incorporating a PEGDE cross-linking agent with a highly carboxylate-functionalized PIM, we developed PCHP to induce dendrite-free, compact Li deposition under high current densities and areal capacities. The designed PCHP demonstrated superior mechanical strength (Young's modulus > 3 GPa) and electrochemical stability. Moreover, the intrinsic ion solvation cages in PCHP increased the Li transference number significantly (t_{Li} = 0.74) and provided efficient Li-ion transfer across the LMA-electrolyte interface. The PCHP@Li anodes demonstrate significant improvements in cycling performance, maintaining high capacity retention and low polarization in full cells paired with high-loading cathodes. This study underscores the critical role of mechanical properties and the electrode-electrolyte interface stability in achieving long-term stability and high reversibility of LMA.

Experimental

Materials and methods. 5,5′,6,6′-Tetrahydroxy-3,3,3′,3′-tetramethyl-1,1′-spirobisindane (TTSBI, >97%, SAMCHEN Chemicals), potassium carbonate (99.99%, Sigma-Aldrich), dimethylformamide (DMF, Alfa Aesar), sodium hydroxide (>98%, Sigma-Aldrich), Poly(ethylene glycol) diglycidyl ether (PEGDE, Sigma-Aldrich), tetrahydrofuran (THF, SAMCHEN Chemicals), methanol (99.5%, SAMCHEN Chemicals) and ethanol (95%, SAMCHEN Chemicals) were used without further purification. Tetrafluoroterephthalonitrile (TFTPN, >98%, Matrix Scientific) was purified by sublimation at 150 °C under low pressure.

Preparation of 3D microporous protective layer. Highly carboxylated PIM (PCH) was synthesized following the methodology outlined in our prior publication.[1] 15g of PIM-1 was placed in a 20% NaOH solution (H_2O/ethanol = 1/1 w/w) and maintained at 125°C for 360 hours (15 days). After cooling, the PCH was immersed in an HCl solution, then washed with DI water until neutralized during filtration. The washed PCH was completely dried, dissolved in THF, precipitated in MeOH, stirred overnight, and finally boiled in fresh MeOH to complete the process. The selected weight ratio of PCH and PEGDE was dissolved in THF solvent, with all mixture concentrations fixed at 12.5 mg mL^{-1}. The mixture was vigorously stirred for 1 h at 40 °C to form a homogeneous solution. The mixture was then drop-cast on 13 mm lithium (Li) metal and dried under Ar gas overnight. Samples consisting of PCH with PEGDE (PCHP) were denoted as PCHP (2:1, wt/wt%), PCHP2 (1:1, wt/wt%), PCHP3 (1:2, wt/wt%) based on the weight ratio.

Material characterization. Proton (^{1}H) Nuclear Magnetic Resonance (NMR) spectra for PCH was acquired using a Bruker AVANCE 500 MHz NMR instrument, with dimethyl sulfoxide-d6 (DMSO-d6) was used for carboxylate-functionalized polymers. To confirm the cross-linking reaction, films made from a mixture of PCH and varying ratios of PEGDE were ground into powder for solid-state NMR analysis (Bruker Avance III HD). Elemental analysis (EA) was performed using a Thermo Scientific FLASH EA-2000 Organic Elemental Analyzer. Nanoindentation (Nano Indenter XP) was performed on each composition coated on glass substrates to evaluate mechanical properties. The crystallinity of PCH and PCHP was investigated using Differential Scanning Calorimetry (DSC, TA instruments Q1000) and X-ray diffraction (XRD, Rigaku Ultima IV) analysis. XRD patterns of the polymers were obtained using equipment with a graphite monochromator and employing Cu Kα radiation (λ = 1.5406 Å) with a scanning range from 10° to 70° at a scanning speed of 1° per minute. Brunauer-Emmett-Teller (BET, Micromeritics) Analysis for CO_2 sorption isotherm at 277K was carried out to examine the microporous characteristics and specific surface area. The morphology of PCHP coated Li was investigated using scanning electron microscopy (SEM, Hitachi SU8230). The top surfaces of cycled PHCP-coated Li and bare Li surfaces were observed using SEM after 50 and 100 cycles in the symmetric Li cell configurations. The chemistry at different layers of PCHP-coated Li surfaces was analyzed by X-ray photoelectron microscopy (XPS, Thermal K-Alpha XPS). High resolution XPS of Li 1s and C 1s were deconvoluted by XPSPEAKS 4.1 software.

Electrode preparation. The $LiNi_{0.83}Mn_{0.06}Co_{0.11}O_2$ (NCM83) cathode was prepared by mixing NCM83 powder, Super P, and PVDF in a weight ratio of 9:0.5:0.5 and coating the mixture onto Al foil. The electrode was then dried in a vacuum oven at 65 ℃ overnight. The active loading density of NCM83 electrode was ~15 mg cm^{-2}. The $LiFePO_4$ (LFP) cathode was prepared in the same manner as the NCM83 electrode, with 9:0.5:0.5 weight ratio. The active loading densities for the LFP cathode were ~16.3 mg cm^{-2} and 23.1 mg cm^{-2}.

Electrochemical measurement. All electrochemical performance tests were conducted using 2032 coin-type cells assembled in an Ar-filled glove box (MBraun, H_2O and O_2 < 0.1 ppm). Celgard 2500 was used as the separator, and 1M $LiPF_6$ in ethylene carbonate (EC):diethyl carbonate (DEC) (1:1, v/v%) with fluoroethylene carbonate (FEC, 10 w/w%) and vinylene carbonate (VC, 1 w/w%) was used as the electrolyte. For the symmetric Li cells, two electrodes (bare Li or PHCP coated Li) were paired to examine the cycling stability. Electrochemical impedance spectroscopy (EIS) was conducted in the frequency range from 300 kHz to 1Hz with a voltage amplitude of 10 mV (Bio Logic VMP3) using Li-Li symmetric cells

with/without the PCHP layer. The conductivity ($C_{polymer}$) was calculated from the given equation below, where resistance ($R_{polymer}$), interlayer thickness (l), and electrode area (A, 1.327 cm^2) are considered.

$$C_{polymer} = \frac{1}{R_{polymer}A}$$

$$R_{polymer} = R_{S,PCHP@Li} - R_{S,Bare\ Li}$$

The steady-state cation transference number was determined by using the Bruce and Vincent method.[2] Full cells were assembled with either a PCHP-coated Li metal anode or a bare Li anode, and the as-prepared cathode. Celgard 2500 and the same electrolyte used in the Li symmetric cell were employed as the separator and electrolyte. A 35 μm thick Li metal anode was used in the full cell with both LFP and NCM83 cathodes. The galvanostatic charge/discharge (GCD) profile and cycling stability were investigated in the potential range of 2.5-4.0 V *vs.* Li^+/Li for LFP and 3.0-4.3 V *vs.* Li^+/Li for NCM83 full cells.

Conflicts of interest

There are no conflicts to declare.

Author Contributions

Kyungbin Lee: Conceptualization, Formal Analysis, Investigation, Data Curation, and writing-original draft. Hyojin Kim: Investigation, Formal Analysis, and writing-original draft. Kun Ryu: Formal Analysis, Methodology. Keun Hee Kim: Formal Analysis, Investigation, and Data Curation. Jun Woo Jeon: Conceptualization, Methodology. Michael J. Lee: Formal Analysis. Soohyun Kim: Resources, validation, Dayoung Kim: Resources, validation, Dongseok Shin: Resources, validation. Byoung Gak Kim: Resources, Conceptualization, Supervision, and Review & Editing. Seung Woo Lee: Resources, Conceptualization, Project Administration, Supervision, Review & Editing.

Data availability

The data that support the plots in this paper and other findings of this study are available from the corresponding author upon reasonable request.

Acknowledgements

This work was supported by LG Energy Solution. This work was performed in part at the Georgia Tech Institute for Electronics and Nanotechnology, a member of the National Nanotechnology Coordinated Infrastructure (NNCI), which is supported by the National Science Foundation (ECCS-2025462). This work was partly supported by the Technology development Program of MSS (s3126915) and Korea Research Institute of Chemical Technology (KRICT) core project (BSF21-112 and KS2422-20).

References

1. D. C. Lin, Y. Y. Liu and Y. Cui, *Nat Nanotechnol*, 2017, **12**, 194-206.
2. Q. Y. Wang, B. Liu, Y. H. Shen, J. K. Wu, Z. Q. Zhao, C. Zhong and W. B. Hu, *Adv Sci*, 2021, **8,** 2101111.
3. W. Deng, X. Yin, W. Bao, X. F. Zhou, Z. Y. Hu, B. Y. He, B. Qiu, Y. S. Meng and Z. P. Liu, *Nat Energy*, 2022, **7**, 1031-1041.
4. C. C. Fang, J. X. Li, M. H. Zhang, Y. H. Zhang, F. Yang, J. Z. Lee, M. H. Lee, J. Alvarado, M. A. Schroeder, Y. Y. C. Yang, B. Y. Lu, N. Williams, M. Ceja, L. Yang, M. Cai, J. Gu, K. Xu, X. F. Wang and Y. S. Meng, *Nature*, 2019, **572**, 511-515.
5. X. D. Ren, L. F. Zou, X. Cao, M. H. Engelhard, W. Liu, S. D. Burton, H. Lee, C. J. Niu, B. E. Matthews, Z. H. Zhu, C. M. Wang, B. W. Arey, J. Xiao, J. Liu, J. G. Zhang and W. Xu, *Joule*, 2019, **3**, 1662-1676.
6. Z. Yu, P. E. Rudnicki, Z. W. Zhang, Z. J. Huang, H. Celik, S. T. Oyakhire, Y. L. Chen, X. Kong, S. C. Kim, X. Xiao, H. S. Wang, Y. Zheng, G. A. Kamat, M. S. Kim, S. F. Bent, J. Qin, Y. Cui and Z. N. Bao, *Nat Energy*, 2022, **7**, 94-106.
7. M. J. Lee, J. Han, K. Lee, Y. J. Lee, B. G. Kim, K.-N. Jung, B. J. Kim and S. W. Lee, *Nature*, 2022, **601**, 217-222.
8. J. Han, M. J. Lee, K. Lee, Y. J. Lee, S. H. Kwon, J. H. Min, E. Lee, W. Lee, S. W. Lee and B. J. Kim, *Adv Mater*, 2023, **35**, 2205194.
9. Z. H. Wu, C. Y. Wang, Z. Y. Hui, H. D. Liu, S. Wang, S. C. Yu, X. Xing, J. Holoubek, Q. S. Miao, H. L. Xin and P. Liu, *Nat Energy*, 2023, **8**, 340-350.
10. W. Chen, Y. Hu, W. Q. Lv, T. Y. Lei, X. F. Wang, Z. H. Li, M. Zhang, J. W. Huang, X. C. Du, Y. C. Yan, W. D. He, C. Liu, M. Liao, W. L. Zhang, J. Xiong and C. L. Yan, *Nat Commun*, 2019, **10**, 4973.
11. Z. Y. Han, C. Zhang, Q. W. Lin, Y. B. Zhang, Y. Q. Deng, J. W. Han, D. C. Wu, F. Y. Kang, Q. H. Yang and W. Lv, *Small Methods*, 2021, **5**, 2001035.
12. Y. Gao, Z. F. Yan, J. L. Gray, X. He, D. W. Wang, T. H. Chen, Q. Q. Huang, Y. G. C. Li, H. Y. Wang, S. H. Kim, T. E. Mallouk and D. H. Wang, *Nat Mater*, 2019, **18**, 384-389.
13. S. M. Li, J. L. Huang, Y. Cui, S. H. Liu, Z. R. Chen, W. Huang, C. F. Li, R. L. Liu, R. W. Fu and D. C. Wu, *Nat Nanotechnol*, 2022, **17**, 613-621.
14. Z. J. Huang, J. C. Lai, S. L. Liao, Z. Yu, Y. L. Chen, W. L. Yu, H. X. Gong, X. Gao, Y. F. Yang, J. Qin, Y. Cui and Z. A. Bao, *Nat Energy*, 2023, **8**, 577-585.
15. X. B. Cheng, R. Zhang, C. Z. Zhao, F. Wei, J. G. Zhang and Q. Zhang, *Adv Sci*, 2016, **3**, 1500213.
16. E. Peled and S. Menkin, *J Electrochem Soc*, 2017, **164**, A1703-A1719.
17. Q. Li, F. L. Zeng, Y. P. Guan, Z. Q. Jin, Y. Q. Huang, M. Yao, W. K. Wang and A. B. Wang, *Energy Storage Mater*, 2018, **13**, 151-159.
18. J. Bae, Y. M. Qian, Y. T. Li, X. Y. Zhou, J. B. Goodenough and G. H. Yu, *Energ Environ Sci*, 2019, **12**, 3319-3327.
19. K. Liu, A. Pei, H. R. Lee, B. Kong, N. Liu, D. C. Lin, Y. Y. Liu, C. Liu, P. C. Hsu, Z. A. Bao and Y. Cui, *J Am Chem Soc*, 2017, **139**, 4815-4820.
20. R. Xu, X. Q. Zhang, X. B. Cheng, H. J. Peng, C. Z. Zhao, C. Yan and J. Q. Huang, *Adv Funct Mater*, 2018, **28**, 1705838.
21. S. Y. Li, L. Fan and Y. Y. Lw, *Energy Storage Mater*, 2019, **18**, 205-212.
22. Y. Y. Liu, D. C. Lin, P. Y. Yuen, K. Liu, J. Xie, R. H. Dauskardt and Y. Cui, *Adv Mater*, 2017, **29**, 1605531.
23. Z. L. Hu, S. Zhang, S. M. Dong, W. J. Li, H. Li, G. L. Cui and L. Q. Chen, *Chem Mater*, 2017, **29**, 4682-4689.
24. R. Xu, Y. Xiao, R. Zhang, X. B. Cheng, C. Z. Zhao, X. Q. Zhang, C. Yan, Q. Zhang and J. Q. Huang, *Adv Mater*, 2019, **31**, 1808392.

25. Y. J. Zhang, G. Y. Wang, L. Tang, J. J. Wu, B. K. Guo, M. Zhu, C. Wu, S. X. Dou and M. H. Wu, *J Mater Chem A*, 2019, **7**, 25369-25376.
26. Y. Zhao, M. Amirmaleki, Q. Sun, C. T. Zhao, A. Codirenzi, L. V. Goncharova, C. H. Wang, K. Adair, X. Li, X. F. Yang, F. P. Zhao, R. Y. Li, T. Filleter, M. Cai and X. L. Sun, *Matter-Us*, 2019, **1**, 1215-1231.
27. L. S. Fan, B. Sun, K. Yan, P. Xiong, X. Guo, Z. K. Guo, N. Q. Zhang, Y. J. Feng, K. N. Sun and G. X. Wang, *Adv Energy Mater*, 2021, **11**, 2102242.
28. F. Liu, Q. F. Xiao, H. B. Wu, L. Shen, D. Xu, M. Cai and Y. F. Lu, *Adv Energy Mater*, 2018, **8**, 1701744.
29. Q. Pang, L. Zhou and L. F. Nazar, *Proc Natl Acad Sci U S A*, 2018, **115**, 12389-12394.
30. A. C. Kozen, C. F. Lin, O. Zhao, S. B. Lee, G. W. Rubloff and M. Noked, *Chem Mater*, 2017, **29**, 6298-6307.
31. M. J. Baran, M. E. Carrington, S. Sahu, A. Baskin, J. Song, M. A. Baird, K. S. Han, K. T. Mueller, S. J. Teat, S. M. Meckler, C. Fu, D. Prendergast and B. A. Helms, *Nature*, 2021, **592**, 225-231.
32. C. Y. Fu, V. Venturi, J. Kim, Z. Ahmad, A. W. Ells, V. Viswanathan and B. A. Helms, *Nat Mater*, 2020, **19**, 758-766.
33. M. J. Baran, M. N. Braten, S. Sahu, A. Baskin, S. M. Meckler, L. Li, L. Maserati, M. E. Carrington, Y.-M. Chiang, D. Prendergast and B. A. Helms, *Joule*, 2019, **3**, 2968-2985.
34. S. E. Doris, A. L. Ward, P. D. Frischmann, L. Li and B. A. Helms, *J Mater Chem A*, 2016, **4**, 16946-16952.
35. J. W. Jeon, D.-G. Kim, E.-h. Sohn, Y. Yoo, Y. S. Kim, B. G. Kim and J.-C. Lee, *Macromolecules*, 2017, **50**, 8019-8027.
36. S. Nameer and M. Johansson, *Journal of Coatings Technology and Research*, 2017, **14**, 757-765.
37. B. Satilmis, M. N. Alnajrani and P. M. Budd, *Macromolecules*, 2015, **48**, 5663-5669.
38. G. H. Moon, H. J. Kim, I. S. Chae, S. C. Park, B. S. Kim, J. Jang, H. Kim and Y. S. Kang, *Chemical Communications*, 2019, **55**, 6313-6316.
39. R. Tan, A. Wang, R. Malpass-Evans, R. Williams, E. W. Zhao, T. Liu, C. Ye, X. Zhou, B. P. Darwich, Z. Fan, L. Turcani, E. Jackson, L. Chen, S. Y. Chong, T. Li, K. E. Jelfs, A. I. Cooper, N. P. Brandon, C. P. Grey, N. B. McKeown and Q. Song, *Nat Mater*, 2020, **19**, 195-202.
40. X. Mei Wu, Q. Gen Zhang, P. Ju Lin, Y. Qu, A. Mei Zhu and Q. Lin Liu, *Journal of Membrane Science*, 2015, **493**, 147-155.
41. Y. Sun, J. Zhang, H. Li, F. Fan, Q. Zhao, G. He and C. Ma, *Separation and Purification Technology*, 2023, **314**, 123623.
42. X. Wang, H. Qiu, C. Yu, Y. Jing, C. Kang, X. Qin, K. Hou, Z. Cui, B. H. Yin and B. Shan, *Separation and Purification Technology*, 2023, **315**, 123723.
43. L. Tian, X. B. Xu, M. Y. Liu, Z. X. Liu and Z. L. Liu, *Langmuir*, 2021, **37**, 3922-3928.
44. J. Evans, C. A. Vincent and P. G. Bruce, *Polymer*, 1987, **28**, 2324-2328.

The data supporting this article have been included as part of the Supplementary Information.